Max-Planck-Institut
für Meteorologie

REPORT No. 163

MODELING BIO-GEOPHYSICAL FEEDBACK IN THE SAHEL

by

MARTIN CLAUSSEN

HAMBURG, May 1995

AUTHORS:

Martin Claußen — Max-Planck-Institut für Meteorologie
Hamburg, Germany

MAX-PLANCK-INSTITUT
FÜR METEOROLOGIE
BUNDESSTRASSE 55
D-20146 HAMBURG
F.R. GERMANY

Tel.: +49 - (0)40 - 411 73 - 0
Telefax: +49 - (0)40 - 411 73 - 298
E-Mail: <name>@dkrz.d400.de

ISSN 0937 – 1060

Modeling bio-geophysical feedback in the Sahel

Martin Claussen

Max-Planck-Institut für Meteorologie

Bundesstr.55

20146 Hamburg, Fed. Rep. Germany

Abstract

An interactively coupled global atmosphere-biome model is used to assess the dynamics of deserts and drought in the Sahel. Under present-day conditions of solar irradiation and sea-surface temperatures, two stable equilibria are found: the first reflects the present-day distribution of vegetation and the second shows a northward spread of savanna and xerophytic shrub of some 600 km, particularly in the south-west Sahara. Comparison of atmospheric states associated with these equilibria corroborates Charney's (Quart.J.R.Met.Soc.,1975) theory of a self-induction of deserts through albedo enhancement.

1 Introduction

Almost three years ago, at a conference on Global Climate Change and Variability, Shukla (1992) gave a review of GCM (general circulation model) response to changes in the boundary conditions at the earth's surface. In particular, Shukla mentioned that 'Charney's cycle' has not yet been close by modellers - referring to Charney's (1975) theory of a positive bio-geophysical feedback of desertification.

Charney (1975) suggested that a desert feeds upon itself in the following manner. Sandy, non-vegetated soil has much higher albedo than soil covered by vegetation. Therefore a desert reflects more solar radiation to space than its vegetated surrounding under the same meteorological conditions. Moreover, desert surfaces are hotter than vegetated surfaces, and the air above is less cloudy. Hence a desert emits more longwave radiation to space. The net result is that a desert is a radiative sink of heat relative to its surroundings. In order to maintain thermal equilibrium, the air must descend and compress adiabatically. Consequently, the relative humidity of the air decreases and the likelihood of precipitation becomes vanishingly small.

This geophysical part of 'Charney's cycle' is understood and has been described in numerical models (see Charney, 1975). What has been missing is the modeling of the response of vegetation to a change in precipitation and, in turn, the response of the atmosphere to a change in vegetation and thereby in land-surface parameters which control the energy, momentum and moisture fluxes at the earth's surface.

Meanwhile, first attempts have been undertaken to incorporate continental vegetation as an interactive component of a global climate model (Henderson-Seller, 1993, Claussen 1994a). The global vegetation scheme used by Henderson-Sellers and by Claussen are diagnostc tools; they are not dynamic models which allow for describing succession of vegetation. Hence the earlier papers as well as this study adresses the equilibrium response of the atmosphere-biosphere system to changes in land-surface conditions.

Claussen (1994a) explored the reaction of a coupled atmosphere-biome model to drastic changes in initial vegetation patterns. He found that parts of the subtropical deserts, particularly the south-west part of the Sahara, become vegetated if the atmosphere-biome model was initialized with a 'green desert'. Claussen (1994a) focussed on the numerical aspects of coupling GCMs with biome models, and his basic result was the

possibility of multiple equilibria of the atmosphere-biome model. These experiments were not ment to provide realistic scenarios.

Here, Claussen's (1994a) experiment is reassessed. Therefore, the atmosphere-biome model, which is briefly presented in the first part of the following section, is set up such that the present-day distribution of global vegetation is a stable solution of the model, i.e. that the present-day distribution of global vegetation can be represented by the model if the model is initialized with this distribution. Then, the atmosphere-biome model is initialized with a drastic change in tropical vegetation, in the following called the 'anomalous initial state'. Subsequently, the atmosphere-biome model is integrated until it finds a new, in the following called 'anomalous' equilibrium. The core of this paper deals with the comparison between present-day and anomalous biome distribution and its associated atmospheric states. It is anticipated that a large-scale change in tropical and subtropcal vegetation induces a response of the Hadley-Walker circulation. Hence the present investigation addresses a global problem. It is not a study of local succession where small-scale, dynamic vegetation model, gap models for example (e.g. Prentice et al., 1993), are the appropriate tools.

2 Atmospheric model and biome model

2.1 The atmospheric model

As atmospheric component of the combined atmosphere-biome model, the climate model ECHAM, developed at the Max-Planck-Institut für Meteorologie in Hamburg, is taken. The model physics as well as its validation is described in detail by Roeckner et al. (1992). In this study, ECHAM is run at T21 resolution, hence the grid at which the vertical transports between the atmosphere and the surface are computed has a resolution of 5.6° × 5.6°, i.e. appr. 600 km × 600km at the equator. The climate model ECHAM (level 3) is able to simulate most aspects of the observed time-mean circulation and its intraseasonal varability with remarkable skill (Roeckner et al., 1992). Nevertheless, there are a few problems. For example, during the respective summer season,

there is too much precipitation over South Africa and Australia and off the west coast of Central America, whereas the rainfall over India is underestimated during the summer monsoon season. There is a lack of precipitation over the Northern Hemisphere continents during summer, for example over the United States, over Europe, and over the dry regions of Asia. In these areas, the boundary-layer temperatures are generally too high with the largest error of about 6K.

In the original version of ECHAM (level 3), there are no specific biomes or vegetation types prescribed. Instead, surface parameters which control the energy, momentum and moisture are specified from topographic or satellite data or are taken as global constants. To allow for coupling with a vegetation model, ECHAM was modified such that arbitrary global data of surface parameters - background albedo, roughness length, vegetation ratio, leaf area index, and forest ratio - can be specified.

2.2 The biome model

Biomes are computed by using the BIOME model of Prentice et al. (1992). Prentice's et al. (1992) model is chosen, because this model is based on physiological considerations rather than on correlations between climate distribution and biomes as they exist today. Biomes are not taken as given as, for instance, in the Holdridge classification, but emerge through the, albeit parameterized, interaction of constituent plants. Therefore, the BIOME model can be applied to the assessment of changes in natural vegetation patterns in response to different climate states. It is important to notice that the BIOME model does not simulate the transient dynamics of vegetation. Hence this is a study of equilibrium-response experiments. How the atmosphere-biosphere system finds its equilibrium is not considered.

In the BIOME model, 14 plant functional types are assigned climate tolerances in terms of amplitude and seasonality of climate variables. For example, the cold tolerance is expressed in terms of the coldest monthly mean temperature and the heat requirement, in terms of yearly temperature sums. The BIOME model predicts which plant functional type can occur in a given environment, i.e. in a given set of climate variables.

Competition between different plant types is treated indirectly by the application of a dominance hierarchy which effectively excludes certain types of plants from a site, based on the presence of others, rather than being excluded by climate (Cramer, 1994). Finally, biomes are defined as combinations of dominant types.

Validation of global biome models is a problem. Using the IIASA climate data base (Leemans and Cramer, 1990), Prentice et al. (1992) predict global patterns of biomes which are in fair agreement with the global distribution of actual ecosystem complexes being evaluated by Olson et al. (1983). Where intensive agriculture has obliterated the natural vegetation, comparison of predicted biomes and observed ecosystems is, of course, omitted.

2.3 Coupling atmospheric model with biome model

The coupling of ECHAM with the BIOME model is done in a rather simple manner, as described in Claussen (1994a). Using monthly means of near-surface temperature, precipitation, and cloudiness produced by ECHAM, the BIOME model evaluates climate constraints mentioned in the previous Section 2.2. Subsequently, a global distribution of biomes is diagnosed by using the same grid as the climate model. From the biome map, a global set of surface parameters, i.e. background albedo α, roughness length z_0, vegetation ratio c_v, leaf area index LAI, and forest ratio c_F, are deduced. With this new set of surface parameters a subsequent integration with ECHAM is performed. (In the following, the sequence of integration and subsequent computation of biomes is also called 'iteration'.)

Based on earlier experience (Claussen, 1994a), each iteration is carried out over several years. Here, a period of six years is chosen. The first year of each period is taken as spin-up time to allow for soil-water transports to adjust. Hence biomes are computed from the climatology of the remaining five years.

Allocation of surface parameters to biomes is mainly based on earlier data found in literature. These data are combined to fit the present biomes. For details see Claussen

(1994a), Claussen et al. (1994). A background albedo α is specified for each biome (as done in the second experiment set up in Claussen, 1994a). The resulting values are listed in Table 1. Likewise, a leaf area index LAI, a forest ratio c_F, and a roughness length of vegetation z_{0v} are allocated to each biome.

	Biome name	α_v	LAI	c_v	c_F	$z_{0v}(m)$
01	tropical rain forest	0.12	9.3	0.98	0.98	2.000
02	tropical seasonal forest	0.12	4.3	0.82	0.82	2.000
03	savanna	0.15	2.6	0.65	0.58	0.361
04	warm mixed forest	0.15	6.0	0.91	0.79	0.716
05	temperate deciduous forest	0.16	2.7	0.65	0.65	1.000
06	cool mixed forest	0.15	2.0	0.54	0.54	1.000
07	cool conifer forest	0.13	9.1	0.97	0.97	1.000
08	taiga	0.14	3.7	0.77	0.77	0.634
09	cold mixed forest	0.15	2.0	0.54	0.54	1.000
10	cold deciduous forest	0.14	3.7	0.77	0.77	0.634
11	xerophytic woods / shrub	0.18	2.6	0.66	0.19	0.111
12	warm grass / shrub	0.20	0.8	0.27	0.00	0.100
13	cool grass / shrub	0.19	1.0	0.33	0.00	0.055
14	tundra	0.17	1.2	0.37	0.06	0.033
15	hot desert	0.20	0.2	0.09	0.00	0.004
16	cool desert	0.20	0.3	0.10	0.00	0.005
17	ice / polar desert	0.15	0.0	0.00	0.00	0.001
18	sand desert	0.35	0.0	0.00	0.00	0.004

Table 1: Allocation of surface parameters used in the climate model to biomes specified in Prentice et al. (1992) BIOME model.

In contrast to Claussen (1994a) the vegetation ratio c_v is not specified, but computed from the empirical relation (see Monteith, 1973)

$$c_v = 1 - exp(-0.4 \times LAI) \quad .$$

In this study, lower values of LAI, but larger values of c_v than in Claussen (1994a) are used. The earlier study of Claussen (1994a) was ment to be a study of (numerical) processes rather than an excercise of predicting realistic global vegetation patterns. Meanwhile, a few integrations were done to find a set of parameters which yields a stable global vegetation patterns: when initializing the ECHAM-BIOME model with a biome distribution close to the present-day biome, then the ECHAM-BIOME model should

not yield a biome distribution which significantly differs from the initial one. (How one can identify significant differences between biome maps is analysed in Claussen, 1994b).

The major improvement of the earlier set of surface parameters in Claussen (1994a) was achieved by adding a new surface type *sand desert* to the original list of biomes. In contrast to *hot desert*, *sand desert* is assumed to have no vegetation at all. Furthermore, and most important, the albedo of *sand desert* is larger than of *hot desert*. The reason for defining an additional biome is the following.

By perturbing the tropical vegetation, Claussen (1994a) tried to explore the consequences of an anomalous initial state on the stability of the ECHAM-BIOME model. By initializing the ECHAM-BIOME model with tropical forests in the place of present-day deserts, and *vice versa*, the ECHAM-BIOME model finds a new equilibrium differing from the present-day global vegetation by a greening of the south-west part of the Sahara and intrusion of desert into India. The unresolved question was whether the former change of vegetation is related to the latter. Meanwhile, it has turned out that the intrusion of desert into India is due to high albedo value ($\alpha = 0.35$) of *hot desert* specified in Claussen (1994a). From satellite data (e.g. Ramanathan et al., 1989), it can be seen that large patches high albedo values (α larger than 0.3) are found only the the interior of the Sahara and the Arabian penninsula. By specifying *sand desert* only in these desert area and *hot desert* otherwise, the equilibrium-response of the ECHAM-BIOME model stays close to the initial present-day biome distribution.

3 The Experiment

3.1 Biomes

Using the ECHAM-BIOME model with the updated allocation of surface parameters to biomes, the problem of multiple equilibria of the atmosphere-biosphere system with respect to vegetation in the Sahel is reassessed. As in the earlier study of Claussen (1994a), the atmospheric model, ECHAM, is is forced by present-day orbital conditions and by the climatology of the annual cycle of SST (sea-surface temperatures) on aver-

age over 1979 to 1988 from the so-called Atmospheric Model Intercomparison Project (AMIP) data set (Gates, 1992). Each run (control run and anomaly run) is started with the same initial atmospheric state which corresponds to the observations of an arbitrary January. Only the initial land-surface conditions are varied.

As mentioned in the previous section, the present-day global biome distribution seems to be a stable one: when initializing the ECHAM-BIOME model with the biome distribution as shown in Figure 1, then the ECHAM-BIOME model yields a biome distribution (shown in Figure 2) which is close to the initial one. The initial biome distribution is computed from the 30-year climatology of the ECHAM climate model. It resembles the biome distribution computed from observed climatology (e.g. Prentice et al., 1992). Differences between biome distribution estimated from simulation and observation are found in some regiones in northern Australia, South Africa, and North America which are related to model deficiencies mentioned in Section 2.1.

The differences between biome distributions of successive iterations as well as between the initial distribution and each iteration period vary in between 12% and 16.5% of the total continental surface area excluding Antarctica. These values are as large as the variability found if biomes are computed from different 5-year climate simulations or better, equally likely numerical realizations, of the same climate state (Claussen 1994a,b)

As in Claussen (1994a), a new equilibrium-response of the ECHAM-BIOME model is sought by perturbing the tropical vegetation such that *hot desert* and *sand desert* is replaced by *tropical rain forest*, and *tropical rain forest*, *tropical seasonal forest*, *savanna*, by *hot desert*, see Figure 3.

With the new, anomalous initial condition, the ECHAM-BIOME "jumps" at a new equilibrium. Biome distributions of all iterations resemble each other. There is no trend in global and individual Kappa statistics when considering differences in biome patterns between successive interations as well as between all interations and the present-day equilibrium distribution. (The Kappa statistics is presented by Monserud and Leemans (1992) as an objective tool for comparing global vegetation maps.) Moreover, there is no trend in land surface covered by each biome. The only exception is *tundra* which only slightly, but significantly expands its total area. The biome distribution resulting

from the 3rd (i.e. last but one) iteration is plotted in Figure 4.

	1	2	3	4	5	6
01	5.42	3.89	1.56	5.05	3.88	3.89
02	4.64	6.16	3.89	4.63	4.63	5.80
03	22.34	23.43	30.73	27.25	26.15	27.28
04	6.16	4.57	4.09	5.25	4.11	5.90
05	4.69	5.44	4.47	5.32	5.02	6.07
06	5.09	5.09	5.37	6.67	4.79	5.42
07	2.81	1.54	2.56	2.73	3.06	2.18
08	11.61	10.03	12.62	13.30	10.80	10.99
09	0.99	1.24	0.99	0.25	1.24	1.24
10	0.50	0.74	1.32	0.80	0.77	0.81
11	12.64	12.53	19.30	14.79	14.82	15.20
12	7.67	6.46	7.63	6.73	9.25	6.13
13	5.98	7.44	5.60	4.18	4.81	4.20
14	15.13	17.34	15.91	16.69	17.12	17.76
15	16.22	16.58	10.89	13.20	14.19	13.06
16	1.87	1.87	0.93	0.63	1.53	1.18
17	7.29	6.69	7.64	6.57	7.14	7.29
18	9.07	9.07	4.62	6.10	6.84	5.73

Table 2: Land surface (in Mio km^2) covered by each biome (for biome numbers see Table 1). Antartica is not included in *polar desert*. Column 1 and 2: results of the atmosphere-biome model initialized with the present-day distribution of vegetation shown in Figure 1. Column 3 to 6: results of successive iterations of the atmosphere-biome model initialized with the anomalous vegetation distribution shown in Figure 3. The biome distribution corresponding to column 2 is shown in Figure 2, that of column 5, in Figure 4.

Table 2 depicts the land surface (in Mio km^2) covered by each biome. (Note that Antartica is not included in *polar desert*.) The first two columns are valid for iterations of the ECHAM-BIOME model when started with the present-day initial condition (column 2 refers to Figure 2). Columns 3 to 6 give the land surface considering the successive iterations started with the anomalous initial condition. From Table 2 it can be inferred that the strongest change occurs for *savanna* (No.3) which increases by approximately 5 Mio km^2 on average over all iterations. *Hot desert* (No.15) and *sand desert* (No.18) decrease by approximately 3.6 Mio km^2 and 3.3 Mio km^2, respectively. *Xerophytic*

woods / shrub (No.11) increases by 3.4 Mio km^2. By comparing Figures 2 and 4, it is obvious that these changes are found at the southern edge of the Sahara, particularly in the south-west part of the Sahara, and Arabian and Indian deserts (the latter concerns only one or two grid boxes). The difference in *cool grass* (No.13) of some 2 Mio km^2 basically concerns Central Asia. By applying a student's t-test it can be shown that the difference in *sand desert* is significant at the 1% level, whereas the differences in *hot desert*, *savanna*, and *cool grass*, at the 5% level. The difference in *xerophytic woods / shrub* cannot be considered significant.

3.2 Atmospheric States

It is not unexpected that the strongest change between present-day and anomalous biome distribution occurs in the Sahel, the border between desert and savanna. Charney (1975) already suggested a self-induction effect of deserts through albedo enhancement which exists when a desert has formed. Since sandy soil has much higher albedo than soil covered by vegetation, a desert reflects more solar radiation to space than its surrounding. Moreover, desert surfaces are hotter than vegetated surfaces, and the air above is less cloudy. Hence a desert emits more longwave radiation to space. The net result is that a desert is a radiative sink of heat relative to its surroundings. This is clearly seen in Figure 5a which depicts the calculated net radiation at the top of the atmosphere for the present-day equilibrium during the summer season JJA (June, July, August). For the other seasons, only slight changes can be observed (not presented here). Figure 5b shows the differences between present-day and anomalous equilibrium indicating an increase of positive net radiation in the Sahara and southern parts of Arabia. There is some decrease of net radiation over Central Africa which is consistent with a northward shift of the Inner Tropical Convergence Zone (ITCZ) (see below). The differences are taken between one control and one anomaly iteration, depicted in Figures 2 and 4, respectively. Other difference plots (between various combinations of control and anomaly iterations) show similar structures, some even a more pronounced decrease of net radiation over Central Africa, and some an increase over the western part of the Indian subcontinent. Hence it is safe to assume that the difference pattern seen in Figure 5 is a consistent difference between normal and anomal equilibrium. Similar

is valid, if the difference between net-radiation at the top of the atmosphere and the energy residuum at the earth's surface is considered (not shown here).

In order to maintain thermal equilibrium, the air above a desert must descend and compress adiabatically. In Figure 6a the simulated present-day velocity potential at 200 hPa on average over the summer season is plotted. The velocity potential indicates the divergent part of the velocity. It is seen that there is a pole of divergence over Indonesia, and a pole of convergence over South Africa. This dipole pattern of the velocity potential indicates the zonal circulation in the tropics. The difference picture (Figure 6b) reveals a shift of this pattern associated with a decrease of convergence above East Africa and an increase of convergence over the tropical Atlantic. The increase of convergence over the West Pacific is found in this difference plot, but not in the others. Hence the latter pattern is not a consistent one. The velocity potential taken at 850 hPa reveals the complementary picture (not shown here) with an increase of convergence of East Africa and a decrease over the tropical Atlantic. Hence this pattern corroborates a shift of descending and ascending (or less descending) motion associated with a shift of vegetation into deserts.

The shift in global circulation patterns, as indicated in the veloctiy potential, influences the formation of high and low pressure systems. Figure 7a shows the prominent patterns during JJA, Aleutian and Azore high presure systems, the low presssure over the Tibetian Plateau, and, on the southern hemisphere, the subtropical high at 30°S and the strom track at approximately 60°S. The difference plot (Figure 7b) reveals complex patterns. By comparison with other difference plots only the decrease of MSLP (mean sea-level pressure) over the Sahara and an increase of MSLP over Tibet remains as a consistent signal. The former coincides with a reduction of the Azore high, not in its strength, but in its extent to the east. (The eastward extension of the Azore high is an unrealistic feature in the ECHAM model.) The strong differences in the southern strom track differ from one realisation to the next which documents the large variability of 5-year means in MSLP.

As a consequence of the shift in MLSP, the pattern of surface wind stress shift as seen in Figures 8a and b. In the control run, the line of convergence of surface wind stress is located at aproximately 12°N in North Africa. (It reaches almost 20° in the

western part of North Africa.) The difference plot, Figure 8b, indicates that the African summer monsoon becomes stronger and reaches farther north in the anomaly run. The second pattern, which remains consistent when comparing the difference between all realizations of the control and anomaly climate, is the deviation of the surface wind pattern over India. The other pattern vary between various realizations.

Monthly means of precipitation (in units mm/month) on average over June, July, August are given in Figure 9a. The ITCZ over Africa as well as the intense rainfall pattern over Indonesia are fairly reproduced by ECHAM. Only the amount of rain over Africa and over India is underestimated (for details see Roeckner et al., 1992) With a north/northeastward shift of vegetation and enhanced African summer monsoon, the rainfall over the SW-Sahara increases by some 100 mm/month (see Figure 9b). Other difference plots also indicate a decrease of precipitation over Upper Guinea where in the control run, a maximum of rainfall is found. This suggests that there is not only an increase in rain over North Africa, but also a north/northeastward shift of the ITCZ. The difference pattern over the Sahel zone is the strongest and most consistent one. Other consistent differences are: a decrease of rain over the tropical Atlantic (not seen in Figure 9b), east of the Philippines, west of Sumatra, an increase of rain over the so-called Empty Quarters, the southern Arabia, over India (the signal south of India is not consistent), over New Guinea. The response of vegetation due to these changes in rainfall are clearly recognized by comparing the biome patterns in Figures 2 and 4 - not over Indonesia where *Tropical Rain Forest* prevails anyhow, but in North Africa, Arabia, and India.

4 Conclusion

The results of this study suggest that under present-day conditions of solar irradiation and sea-surface temperatures, at least two stable equilibria of the ECHAM-BIOME model are possible: the present-day and an anomalous equilibrium. The former is associated with the present-day distribution of vegetation and the latter with savanna and

xerophytic shrub in the southern part of the Sahara and Arabian and Indian deserts, all else being similar. The difference between biome patterns are caused by a change in the radiation budget of the air above the 'green desert' and by a subsequent change in large-scale vertical motion and shift of the ITCZ. This is in keeping with Charney's (1975) proposal. The question remains whether the existence of two equilibria is realistic.

Validation by large-scale experiments is certainly unwarranted. Simulation of past climates using the ECHAM-BIOME model could give some clues. This will be done in next future. Hence it remains to be critically assessed whether the assumptions which the ECHAM-BIOME model is based on are realistic.

One *caveat* is that the biome model is a static model. The ECHAM-BIOME model cannot deal with transient vegetation dynamics, it merely predicts equilibrium states. Hence the ECHAM-BIOME model does not tell how the vegetation intrudes into deserts. If such an intrusion is unlikely to happen under present-day conditions, then it seems hardly possible that the anomalous equilibrium state will occur in reality. Careful analysis of vegetation in North Africa reveals that the boundaries of the Sahara appear rather stable for the last 130 years (Schulz and Hagedorn, 1994). On the other hand, there is evidence from paleo-climatological records that the vegetation in the Sahara has changed during the Holocene (e.g. Crowley and North, 1991, 68 pp.).

Secondly, the ECHAM-BIOME model allows for changes in vegetation structure only, changes in soil properties are not taken into account. This limitation is serious if changes in tropical rain forest are considered. In the rain forest, the largest portion of the biomass is found in the plants and only little in the soil. Deforestation of rain forest necessarily implies degradation of soil. Therefore, the stability of rain forest in this ECHAM-BIOME model - *tropical rain forest* and *tropical seasonal forest* is predicted to occur under present-day as well as under anomalous conditions - is questionable. Artificial aforestation of deserted regions, on the other hand, seems feasable. A sensitivity study of the influence of soil properties on the ECHAM-BIOME model will be undertaken as soon as the new version of ECHAM, ECHAM level 4, is coupled to the BIOME model. ECHAM-4 allows for a more realistic treatment of soil temperature and soil water transport. Within this context, also the problem of defining the new biome *sand desert* from climate and soil constraints will be readdressed. (So far, definition of *sand*

desert in terms of moisture availability only has not been successful.) Here, *sand desert* was merely prescribed using satellite data.

Thirdly, there is no response of the ocean in the ECHAM-BIOME model. Since Lamb and Peppler (1992) found a correlation between sub-Saharan rain fall and SST of the tropical Atlantic, one cannot exclude that there is a feedback between ocean dynamics and large-scale vegetation changes. On the other hand, the results obtained from a coupled atmosphere-ocean GCM by Hoffmann et al. (1995) show just marginal effects of tropical deforestation on the large-scale air-sea interaction. The latter result is certainly suggestive, but not conclusive, hence more experimentation must be done.

The main conclusion of this paper is that an equilibrium-response atmosphere-biome model reveals multiple equilibria, thus confirming the basic result of an earlier study (Claussen, 1994a) with a less realistic allocation of land surface parameters to biomes. The above mentioned *caveats* do not reveal serious draw backs of the present study, rather they indicate the direction further research has to follow.

Acknowledgements

The author would like to thank Colin Prentice, Dept. of Plant Ecology, Lund University, Sweden, for making the BIOME model available. Thanks are also due to Claudia Kubatzki, Universität Hamburg, for programming assistance.

References

Charney, J. G. (1975) Dynamics of deserts and drought in the Sahel. Quart. J. R. Met. Soc. 101: 193-202.

Claussen, M. (1994a). Coupling global biome models with climate models. Climate Res. 4: 203-221.

Claussen, M. (1994b). Variability of global biome patterns as function of initial and boundary conditions in a climate model Climate Dyn. submitted

Claussen, M., Esch, M. (1994). Biomes computed from simulated climatologies. Climate Dyn. 9: 235-243

Claussen, M., Lohmann, U., Roeckner, E., Schulzweida, U. (1994). A global data set of land-surface parameters. Report 135 Max-Planck-Institut für Meteorologie, Hamburg, F.R.G.

Cramer W (1994) Using plant functional types in a global vegetation model. In: Smith TM, Shugart HH, Woodward FI (eds.) (forthcoming) Plant Funtional Types. Cambridge University Press, Cambridge, England.

Crowley, T.J., North, R.N. (1991) Paleoclimatology. Oxford Monographs on Geology and Geophysics No. 18, Oxford University Press, New York.

Gates, W.L. (1992). AMIP: The atmospheric model intercomparison project. Bull. Amer. Meteor. Soc. 73: 1962-1970.

Henderson-Sellers, A. (1993). Continental vegetation as a dynamic component of global climate model: a preliminary assessment. Climatic Change 23: 337-378

Hoffmann, G., Claussen, M., Latif, M., Stockdale, T. (1995). Does tropical deforestation affect large-scale air-sea interactions? J. Climate, submitted.

Lamb, P.J. and Peppler, R.A. (1992) Further case studies of tropical Atlantic surface atmospheric and oceanic patterns associated with sub-Saharan drought. J. Climate 5: 476-487.

Leemans, R., Cramer, W. (1991). The IIASA database for mean monthly values of temperature, precipitation, and cloudiness on a global terrestrial grid. IIASA Research Report RR-91-18, Laxenburg, Austria

Monserud, R. A., Leemans, R. (1992). Comparing global vegetation maps with Kappa statistic. Ecological Modelling 62: 275-293

Monteith, J.R. (1973) Principals of Enviromental Physics, 141 p., Elsevier, New York.

Olson, J. S., Watts, J. A., Allison, L. J. (1983). Carbon in live vegetation of major world ecosystems. ORNL-5862, Oak Ridge National Laboratory, Oak Ridge

Prentice, I. C., Cramer, W., Harrison, S. P., Leemans, R., Monserud, R. A., Solomon, A. M. (1992). A global biome model based on plant physiology and dominance, soil properties and climate. Journal of Biogeography 19: 117-134

Roeckner, E., Arpe, K., Bengtsson, L., Brinkop, S., Dümenil, L., Kirk, E., Lunkeit, F., Esch, M., Ponater, M., Rockel, B., Sausen, R., Schlese, U., Schubert, S., Windelband, M. (1992). Simulation of the present-day climate with the ECHAM model: Impact of model physics and resolution. Report 93, Max-Planck-Institut für Meteorologie, Hamburg

Schulz, E. and Hagedorn, H. (1994) Die Wüste - wächst sie denn wirklich? Geowissenschaften 12:, 204-212

Shukla, J. (1992) GCM response to changes in the boundary conditions at the earth's surface: a review. in: Second International Conference on Modelling of Global Climate Change and Variability, Abstracts. Max-Planck-Institut für Meteorologie, Hamburg, p. 52

Figure 0: Key to colors used for biomes in Figures 1-4.

Figure 1: Biome distribution computed from a 30 year simulation of the present-day climate with the Hamburg climate model ECHAM 3.

Figure 2: Equilibrium response of the atmosphere-biome model initialized with the present-day biome distribution shown in Figure 1. The area (in Mio km^2) covered by each biome is listed in Table 2 column 2.

Figure 3: Anomalous initial biome distribution.

Figure 4: Equilibrium response of the atmosphere-biome model initialized with the anomalous biome distribution shown in Figure 3. The area (in Mio km^2) covered by each biome is listed in Table 2 column 5.

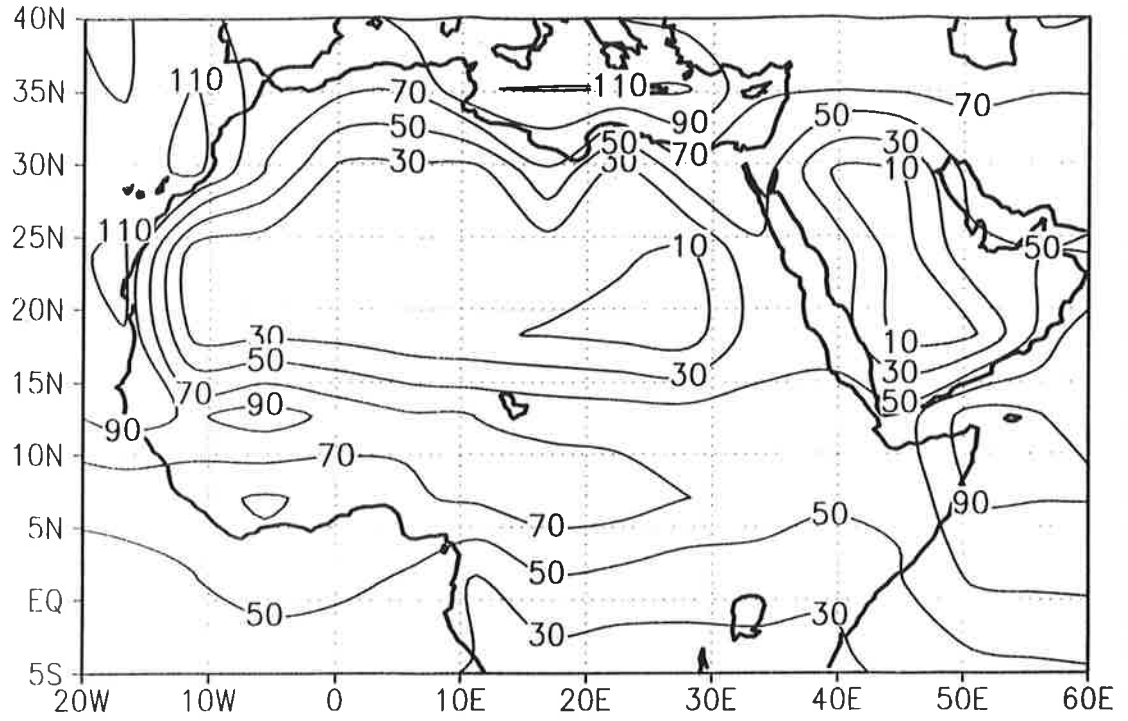

Figure 5a: Net radiation (in W/m^2) at the top of the atmosphere computed with the atmosphere-biome model initialized with present-day vegetation distribution. The corresponding biome distribution is shown in Figure 2.

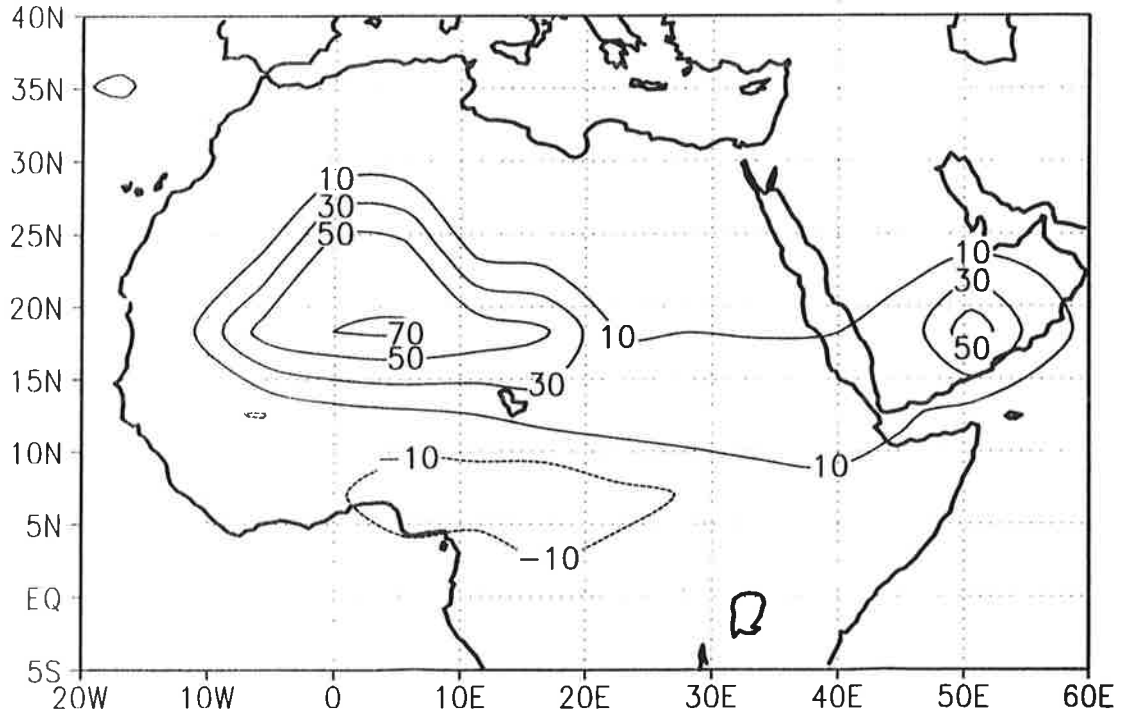

Figure 5b: Difference in net radiation (in W/m^2) between the two equilibrium solutions of the atmosphere-biome model. These solutions are obtained by initializing the atmosphere-biome model with the present-day biome distribution (Figure 1) and the anomalous biome distribution (Figure 3), respectively. The corresponding biome distributions are shown in Figures 2 and 4.

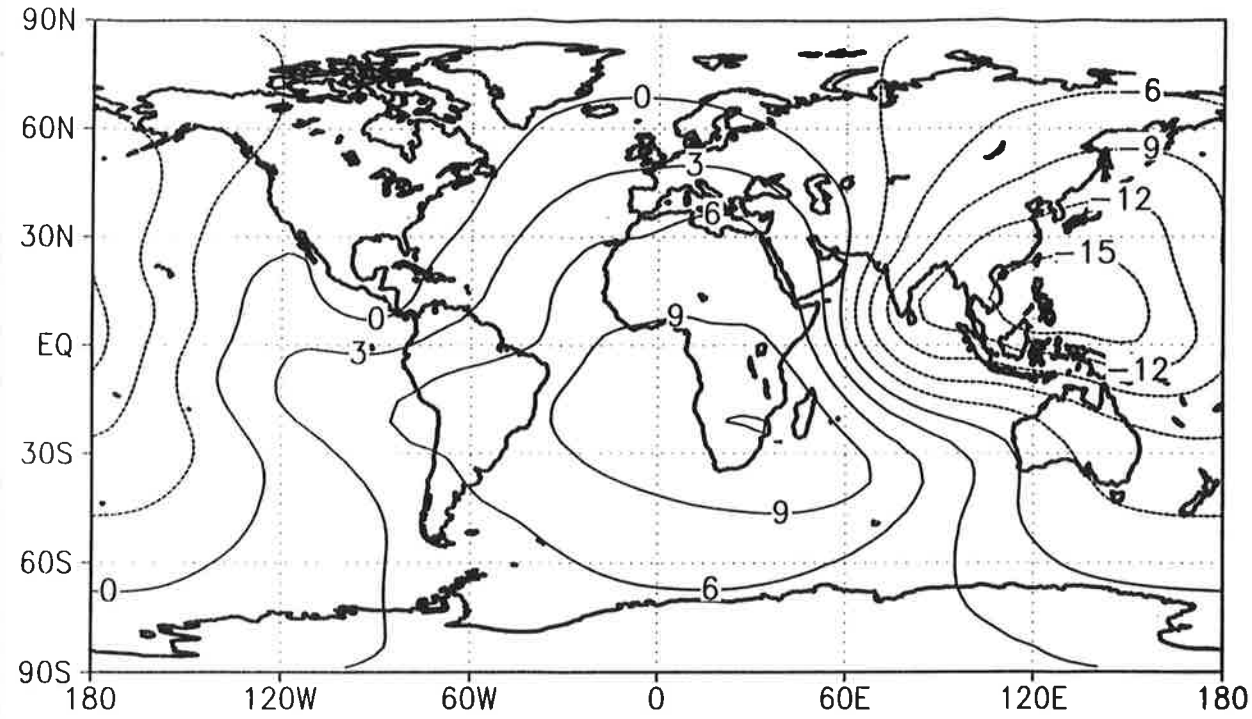

Figure 6a: Same as Figure 5a, except for the velocity potential (in km^2/s) at 200 hPa. The velocity potential is a measure for the divergent part of the large-scale velocity.

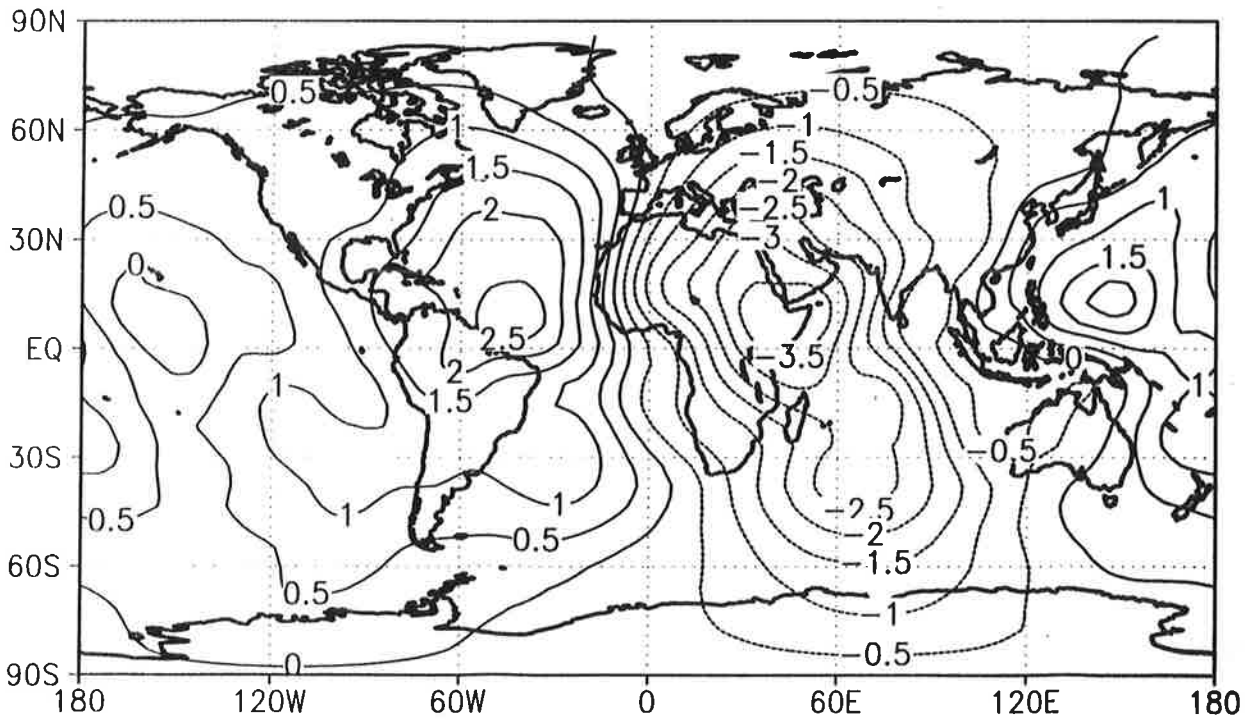

Figure 6b: Same as Figure 5b, except for differences in velocity potential.

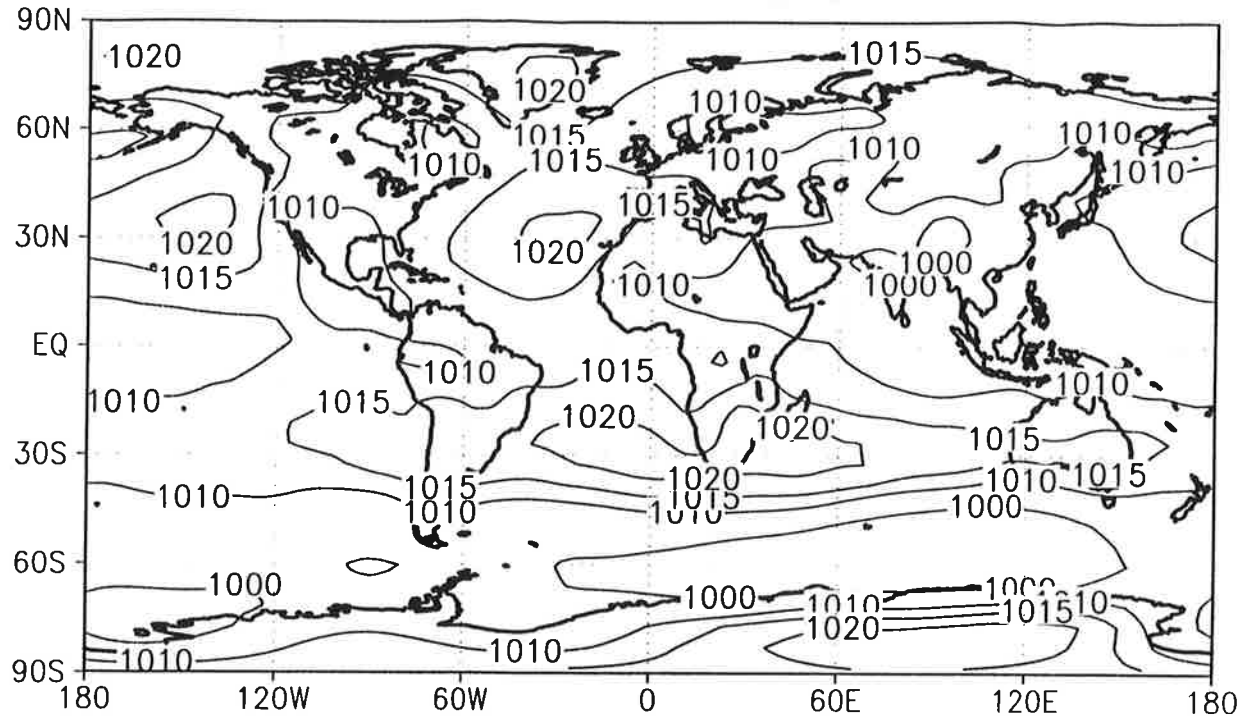

Figure 7a: Same as Figure 5a, except for mean sea level pressure (in hPa).

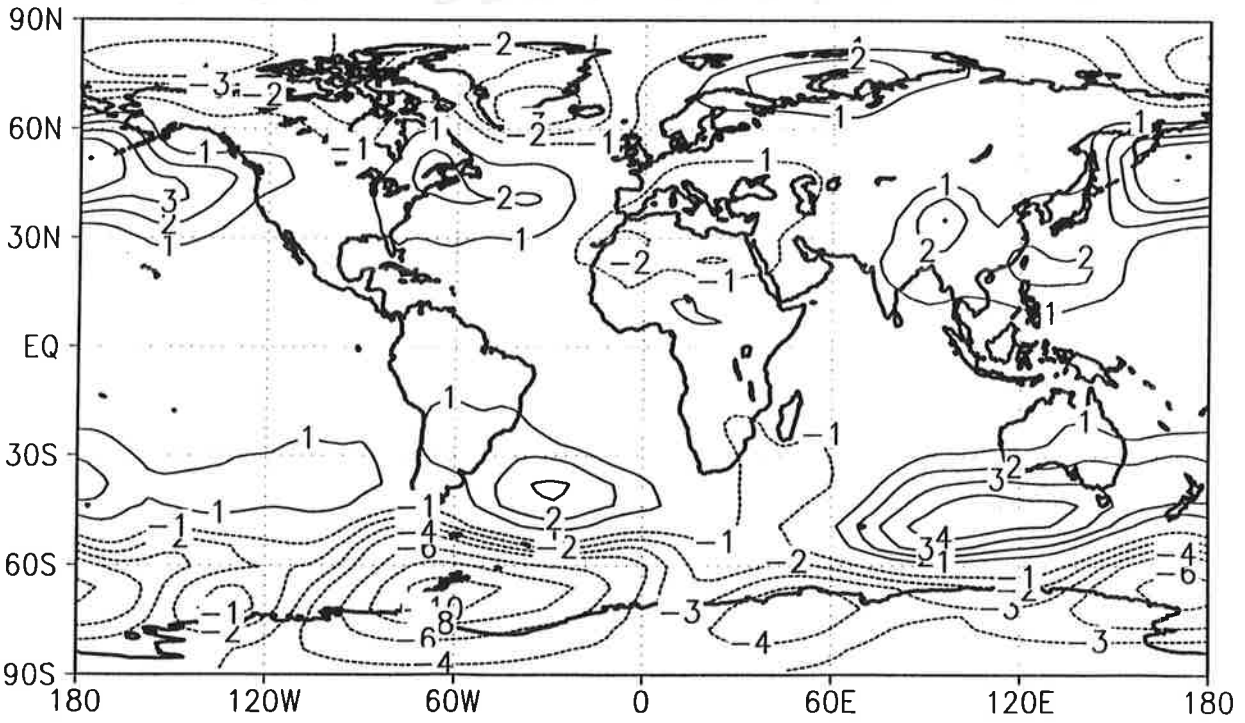

Figure 7b: Same as Figure 5b, except for differences in mean sea level pressure.

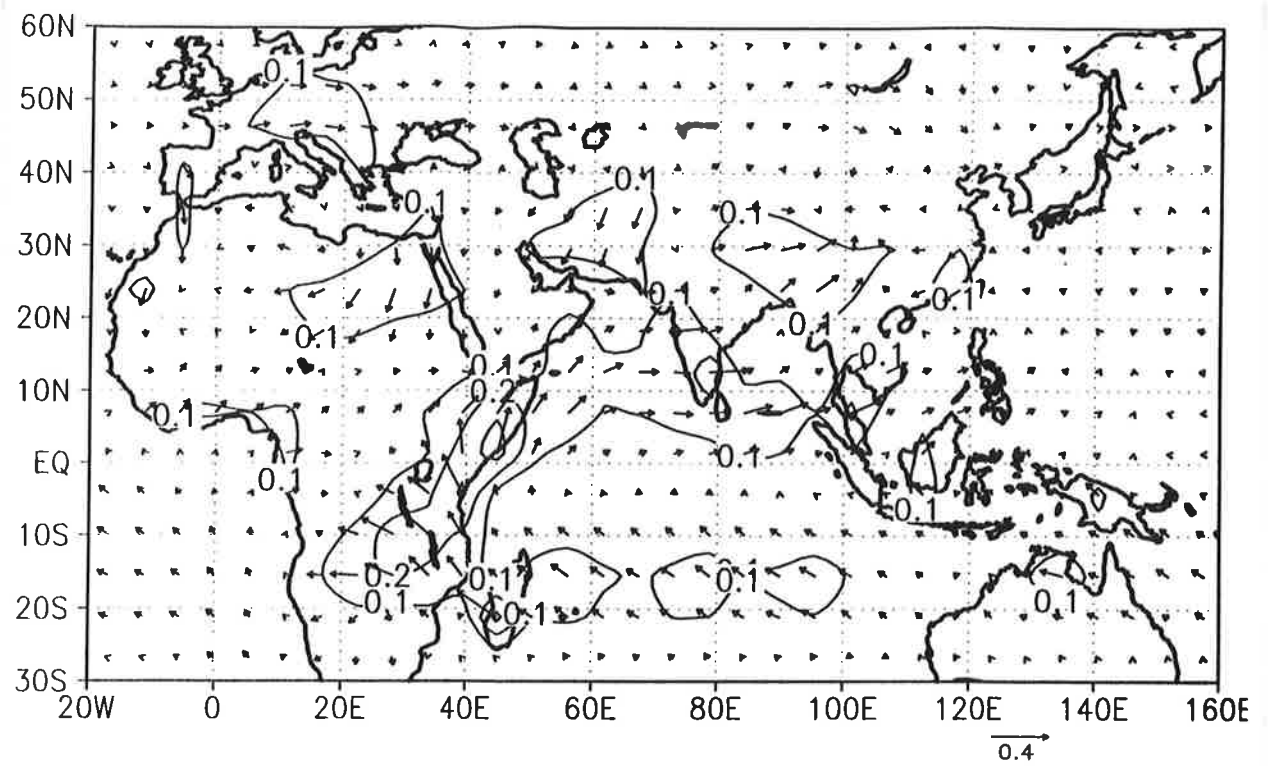

Figure 8a: Same as Figure 5a, except for surface wind stress (in mN/m^2). Shown are amplitude and direction of wind stress.

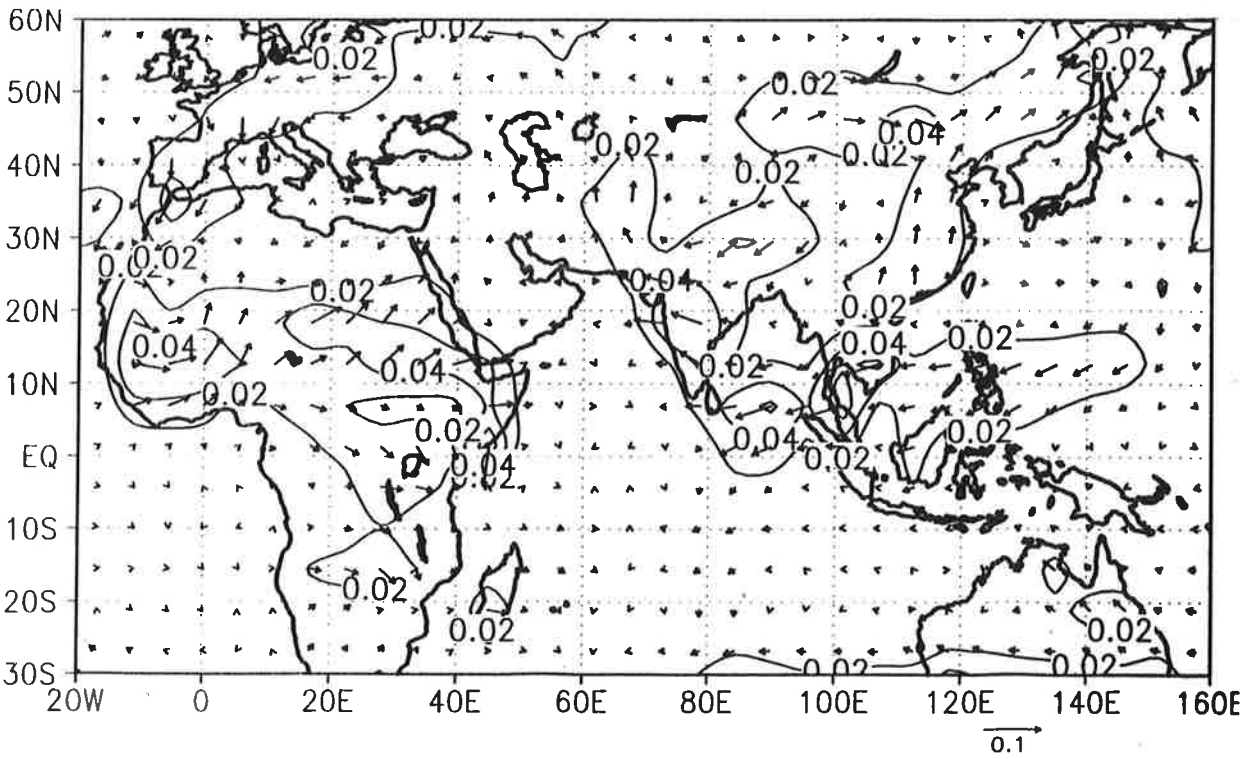

Figure 8b: Same as Figure 5b, except for differences in surface wind stress.

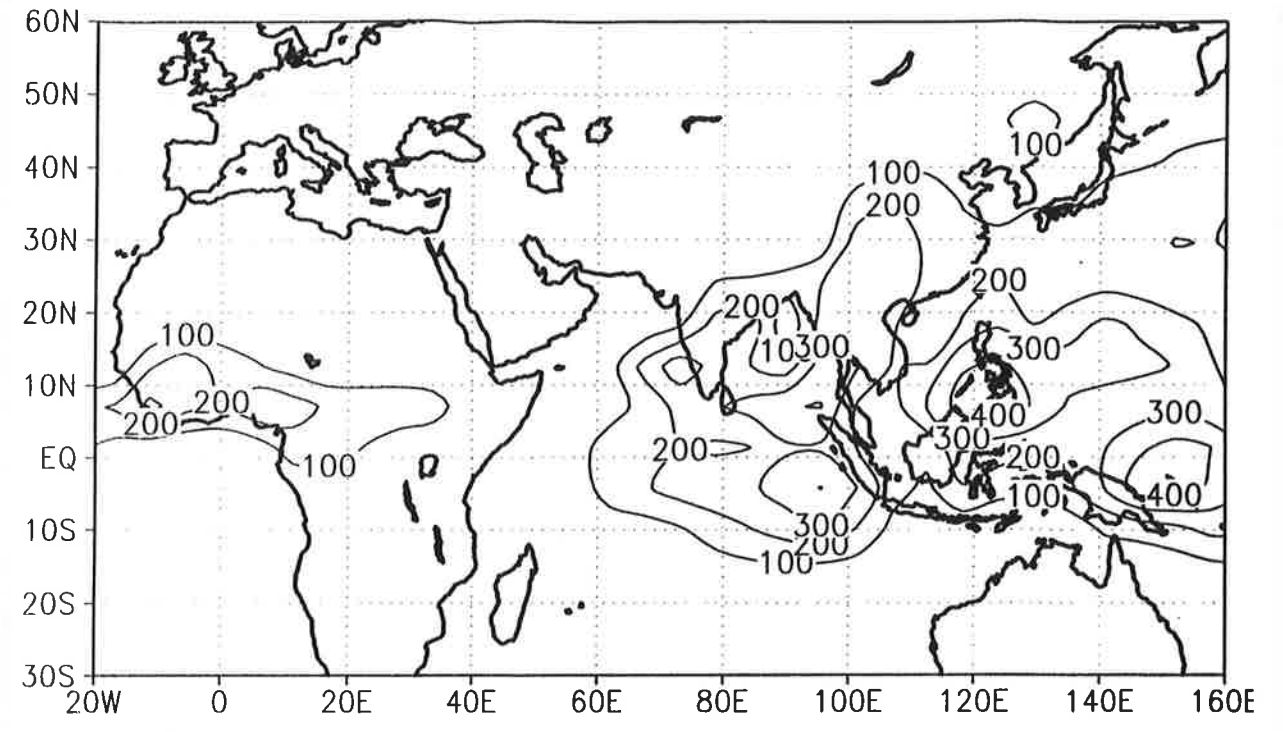

Figure 9a: Same as Figure 5a, except for precipitation (in mm/month).

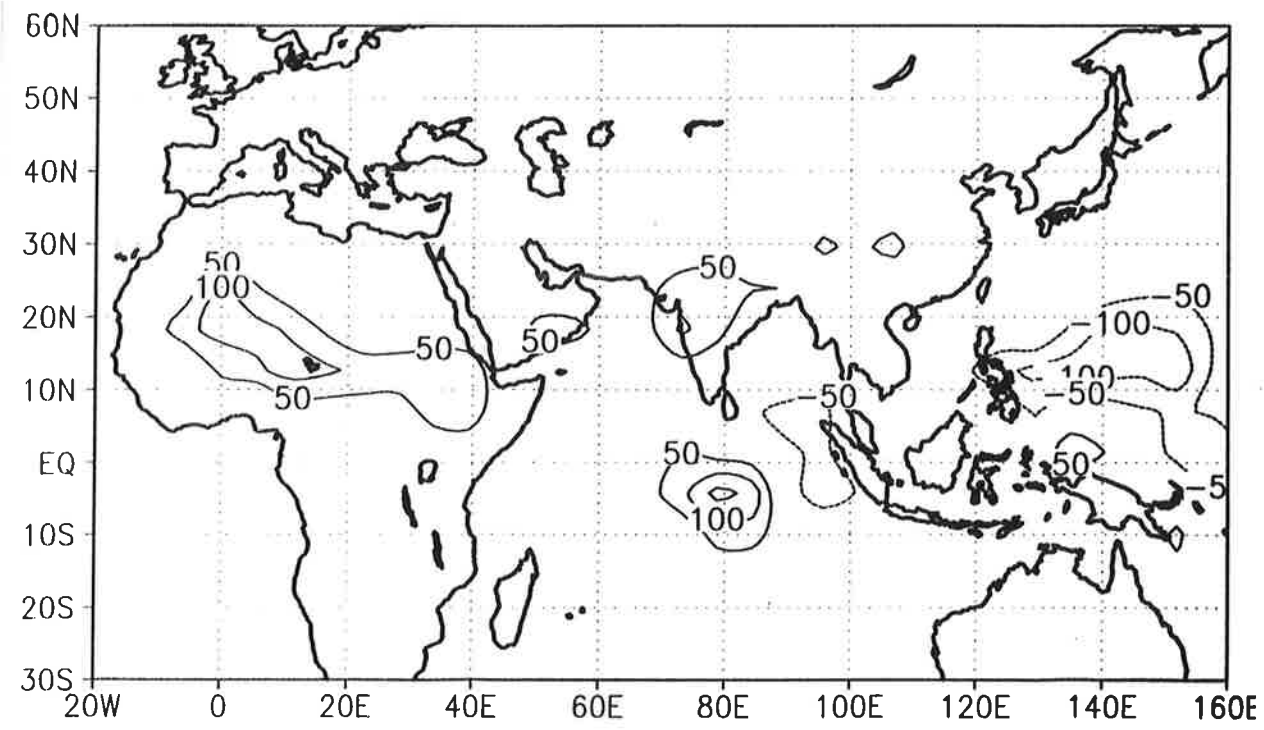

Figure 9b: Same as Figure 5b, except for differences in precipitation.